

## Supporting Information

### A Triangular Dy<sub>3</sub> Single-Molecule Toroic with High Inversion Energy Barriers: Magnetic Properties and Multiple Steps Assembly Mechanism

Zhong-Hong Zhu,<sup>1</sup> Xiong-Feng Ma,<sup>1</sup> Hai-Ling Wang,<sup>1</sup> Hua-Hong Zou,<sup>\*,1</sup> Kai-Qiang Mo,<sup>1</sup> Yi-Quan Zhang<sup>\*,2</sup> Qi-Zhen Yang,<sup>1</sup> Bo Li,<sup>\*,3</sup> Fu-Pei Liang,<sup>\*,1,4</sup>

<sup>1</sup>State Key Laboratory for Chemistry and Molecular Engineering of Medicinal Resources, School of Chemistry & Pharmacy of Guangxi Normal University, Guilin 541004, P. R. China. E-mail: fliangoffice@yahoo.com, gxnuchem@foxmail.com

<sup>2</sup>Jiangsu Key Laboratory for NSLSCS, School of Physical Science and Technology, Nanjing Normal University, Nanjing 210023, P. R. China. E-mail: zhangyiquan@nynu.edu.cn

<sup>3</sup>College of Chemistry and Pharmaceutical Engineering, Nanyang Normal University, Nanyang 473061, P. R. China. E-mail: libozzu0107@163.com

<sup>4</sup>Guangxi Key Laboratory of Electrochemical and Magnetochemical Functional Materials, College of Chemistry and Bioengineering, Guilin University of Technology, Guilin 541004, P. R. China

Supporting Tables	
<b>Table S1</b>	Crystallographic data of the complex <b>1</b> .
<b>Table S2</b>	Selected bond lengths (Å) and angles (°) of <b>1</b> .
<b>Table S3a~3c</b>	<i>SHAPE</i> analysis of the Dy <sup>I</sup> (III), Dy <sup>II</sup> (III) and Dy <sup>III</sup> (III) ions for complex <b>1</b> .
<b>Table S3d</b>	Ranges of bond lengths and angles for <b>1</b> .
<b>Table S4</b>	Hirshfeld surfaces mapped with $d_{norm}$ (left) showing Shape-index (middle) and Curvedness (right) for the <b>1</b> . Hirshfeld surface analysis were performed using CrystalExplorer (Version 3.1), S. K. Wolff, D. J. Grimwood, J. J. McKinnon, M. J. Turner, D. Jayatilaka, M. A. Spackman, University of Western Australia, 2012.
<b>Table S5</b>	Fingerprint plot for different interactions for <b>1</b> showing the percentage of contacts created to the total Hirshfeld surface area of the <b>1</b> molecules. $d_i$ is the closest internal distance from a given point on the Hirshfeld surface; $d_e$ is the closest external contact.
<b>Table S6</b>	Selected parameters from the fitting result of the Cole-Cole plots for <b>1</b> under 0 Oe field.
<b>Table S7</b>	Magneto-structural data for triangular Dy <sub>3</sub> SMMs.
<b>Table S8</b>	Calculated energy levels (cm <sup>-1</sup> ), $g$ ( $g_x$ , $g_y$ , $g_z$ ) tensors and $m_J$ values of the lowest eight Kramers doublets (KDs) of individual Dy <sup>III</sup> fragments.

<b>Table S9</b>	Wave functions with definite projection of the total moment $ m_J\rangle$ for the lowest three Kramers doublets (KDs) of individual Dy <sup>III</sup> fragments.
<b>Table S10</b>	Exchange energies (cm <sup>-1</sup> ) and main values of the $g_z$ for the lowest four exchange doublets of complex <b>1</b> .
<b>Table S11</b>	Major species assigned in the ESI-MS of <b>1</b> in positive mode.
<b>Table S12</b>	Major species assigned in the ESI-MS of <b>1</b> in negative mode.
<b>Table S13</b>	Major species assigned in the Time-dependent ESI-MS of <b>1</b> in positive mode.
<b>Supporting Figures</b>	
<b>Figure S1a</b>	(a) The structure after the coordination of nitrate was removed; (b) Only the structure located in the equatorial plane was retained; (c) The structure after the removal of the equatorial plane ligands; (d) Structure of <b>1</b> showing the supramolecular interactions.
<b>Figure S1b</b>	Thermogravimetry of the compounds data heating rate of 5 °C/min under N <sub>2</sub> atmosphere for <b>1</b> .
<b>Figure S2</b>	Temperature dependence of $\chi_m T$ (a) Field dependence of the magnetization; (b) for <b>1</b> .
<b>Figure S3</b>	Calculated model structure of Dy <sup>III</sup> fragment of <b>1</b> (Dy1) of complex <b>1</b> ; H atoms are omitted.
<b>Figure S4</b>	Magnetization blocking barriers for individual Dy <sup>III</sup> fragments of <b>1</b> (Dy1), <b>1</b> (Dy2) and <b>1</b> (Dy3) in complex <b>1</b> . The thick black lines represent the Kramers doublets as a function of their magnetic moment along the magnetic axis. The green lines correspond to diagonal quantum tunneling of magnetization (QTM); the blue line represent off-diagonal relaxation process. The numbers at each arrow stand for the mean absolute value of the corresponding matrix element of transition magnetic moment.
<b>Figure S5</b>	Three types of $J_1$ , $J_2$ and $J_3$ in complex <b>1</b> .
<b>Figure S6</b>	Calculated (red solid line) and experimental (black circle dot) data of magnetic susceptibility of complex <b>1</b> . The intermolecular interactions $zJ'$ of complex <b>1</b> was fitted to $-0.30$ cm <sup>-1</sup> .
<b>Figure S7</b>	Positive ESI-MS spectra of <b>1</b> in DMF (In-Source CID 0, 20, 40, 60, 80 eV).
<b>Figure S8</b>	The superposed simulated and observed spectra of several species for <b>1</b> (In-Source CID 0 eV).
<b>Figure S9</b>	The superposed simulated and observed spectra of several species for <b>1</b> (In-Source CID 20 eV).
<b>Figure S10</b>	The superposed simulated and observed spectra of several species for <b>1</b> (In-Source CID 40, 60 and 80 eV).
<b>Figure S11</b>	Negative ESI-MS spectra of <b>1</b> in DMF (In-Source CID 0, 20, 40, 60, 80 eV).
<b>Figure S12</b>	The superposed simulated and observed spectra of several species for <b>1</b> (In-Source CID 0 eV).
<b>Figure S13</b>	The superposed simulated and observed spectra of several species for <b>1</b> (In-Source CID 20 eV).
<b>Figure S14</b>	The superposed simulated and observed spectra of several species for <b>1</b> (In-Source CID 40, 60 and 80 eV).
<b>Figure S15</b>	ESI-MS at different times during the reaction from HL and Dy(NO <sub>3</sub> ) <sub>3</sub> ·6H <sub>2</sub> O under ambient conditions.
<b>Figure S16</b>	The time-dependent ESI-MS superposed simulated and observed spectra of several species for <b>1</b> .

**Table S1.** Crystallographic data of the complex1.

<b>Complex</b>	<b>1</b>
Formula	C <sub>46</sub> H <sub>45</sub> Dy <sub>3</sub> N <sub>14</sub> O <sub>18</sub>
Formula weight	1569.46
<i>T</i> (K)	293(2)
Crystal system	Triclinic
Space group	<i>P</i> -1
<i>a</i> (Å)	12.6762(9)
<i>b</i> (Å)	13.0303(4)
<i>c</i> (Å)	19.2205(10)
<i>α</i> (°)	101.791(4)
<i>β</i> (°)	101.667(5)
<i>γ</i> (°)	111.029(2)
<i>V</i> (Å <sup>3</sup> )	2765.7(2)
<i>Z</i>	2
<i>D<sub>c</sub></i> (g cm <sup>-3</sup> )	1.885
<i>μ</i> (mm <sup>-1</sup> )	4.094
Reflns coll.	21194
Unique reflns	10837
<i>R</i> <sub>int</sub>	0.0366
<sup>a</sup> <i>R</i> <sub>1</sub> [ <i>I</i> ≥ 2σ( <i>I</i> )]	0.0504
<sup>b</sup> <i>wR</i> <sub>2</sub> (all data)	0.1426
GOF	1.050

$$^a R_1 = \frac{\sum ||F_o| - |F_c||}{\sum |F_o|}, \quad ^b wR_2 = \left[ \frac{\sum w(F_o^2 - F_c^2)^2}{\sum w(F_o^2)^2} \right]^{1/2}.$$

**Table S2.** Selected bond lengths (Å) and angles (°) of complex **1**.

<b>Bond lengths (Å)</b>					
Dy1—O1	2.297 (5)	Dy2—N3	2.541 (7)	Dy3—O2	2.336 (6)
Dy1—O3	2.491 (6)	Dy2—O1	2.301 (5)	Dy3—O3	2.421 (5)
Dy1—O4	2.500 (5)	Dy2—O2	2.305 (5)	Dy3—O4	2.398 (5)
Dy1—O5	2.313 (5)	Dy2—O3	2.404 (5)	Dy3—O5	2.295 (6)
Dy1—O8	2.520 (6)	Dy2—O4	2.425 (6)	Dy3—N5	2.430 (7)
Dy1—N1	2.530 (6)	Dy2—O13	2.480 (6)	Dy3—N9	2.539 (7)
Dy1—O6	2.497 (7)	Dy2—O12	2.449 (7)	Dy3—O15	2.486 (5)
Dy1—O11	2.501 (7)	Dy2—N7	2.459 (7)	Dy3—O16	2.441 (6)
Dy1—O9	2.521 (7)				
<b>Bond angles (°)</b>					
O2—Dy3—O3	73.71 (18)	O3—Dy3—N5	68.58 (19)	O4—Dy3—N9	132.4 (2)
O2—Dy3—O4	69.60 (19)	O3—Dy3—N9	123.05 (19)	O4—Dy3—O15	126.7(2)
O2—Dy3—N5	80.0 (2)	O3—Dy3—O15	143.8 (2)	O4—Dy3—O16	84.78 (19)
O2—Dy3—N9	155.3 (2)	O3—Dy3—O16	147.25 (19)	O5—Dy3—O2	137.0 (2)
O2—Dy3—O15	78.83 (19)	O4—Dy3—O3	63.75 (18)	O5—Dy3—O3	72.14 (19)
O2—Dy3—O16	87.5 (2)	O4—Dy3—N5	128.7 (2)	O5—Dy3—O4	72.23 (19)
N5—Dy3—N9	89.5 (2)	O15—Dy3—N9	77.9 (2)	O5—Dy3—N5	110.2 (2)
N5—Dy3—O15	84.0 (2)	O16—Dy3—N9	84.3 (2)	O5—Dy3—N9	67.6 (2)
N5—Dy3—O16	135.2 (2)	O16—Dy3—O15	51.3 (2)	O5—Dy3—O15	142.1 (2)
O1—Dy1—O3	72.28 (19)	O3—Dy1—O4	61.31 (18)	O5—Dy3—O16	108.1 (2)
O1—Dy1—O4	71.08 (18)	O3—Dy1—O8	75.44 (19)	O4—Dy1—O8	132.0 (2)
O1—Dy1—O5	135.5 (2)	O3—Dy1—N1	133.8 (2)	O4—Dy1—N1	122.7(2)
O1—Dy1—O8	77.1 (2)	O3—Dy1—O6	93.8 (2)	O4—Dy1—O9	118.0 (2)
O1—Dy1—N1	67.9 (2)	O3—Dy1—O9	146.40 (19)	O4—Dy1—O11	75.4 (2)
O1—Dy1—O6	126.5 (2)	O3—Dy1—O11	135.7 (2)	O5—Dy1—O3	70.59 (19)
O1—Dy1—O9	141.2 (2)	O6—Dy1—O4	145.6 (2)	O5—Dy1—O4	70.08 (18)
O1—Dy1—O11	103.5 (2)	O6—Dy1—O8	49.5 (2)	O5—Dy1—O8	115.4 (2)
O8—Dy1—N1	73.7 (2)	O6—Dy1—N1	91.5 (2)	O5—Dy1—N1	155.0 (2)
O8—Dy1—O9	109.3 (2)	O6—Dy1—O9	69.0 (2)	O5—Dy1—O6	79.7 (2)
O9—Dy1—N1	77.2 (2)	O6—Dy1—O11	119.8 (3)	O5—Dy1—O9	77.8 (2)
O11—Dy1—O8	148.2 (2)	O1—Dy2—N3	153.9 (2)	O5—Dy1—O11	86.9 (2)
O11—Dy1—N1	77.2 (2)	O1—Dy2—O2	138.44 (19)	O2—Dy2—N3	67.3 (2)
O11—Dy1—O9	50.8 (2)	O1—Dy2—O3	73.87 (18)	O2—Dy2—O3	74.58 (18)
O3—Dy2—N3	127.4 (2)	O1—Dy2—O4	72.44 (18)	O2—Dy2—O4	69.62 (19)
O3—Dy2—O4	63.61 (19)	O1—Dy2—O13	78.3 (2)	O2—Dy2—O13	143.1 (2)
O3—Dy2—O13	126.6 (2)	O1—Dy2—O12	89.2 (2)	O2—Dy2—O12	113.1 (2)
O3—Dy2—O12	83.2 (2)	O1—Dy2—N7	81.6 (2)	O2—Dy2—N7	100.4 (2)

O3—Dy2—N7	131.9 (2)	O4—Dy2—N3	128.0 (2)	O13—Dy2—N3	76.4 (2)
Dy2—O2—Dy3	100.9 (2)	O4—Dy2—O13	144.3 (2)	O12—Dy2—N3	80.0 (2)
Dy3—O4—Dy1	95.74 (19)	O4—Dy2—O12	145.2 (2)	O12—Dy2—O13	51.5 (2)
Dy3—O4—Dy2	95.9 (2)	O4—Dy2—N7	69.8 (2)	O12—Dy2—N7	137.8 (2)
Dy3—O5—Dy1	104.1 (2)	Dy3—O3—Dy1	95.4 (2)	N7—Dy2—N3	90.6 (2)
Dy2—O3—Dy1	94.76 (19)	Dy2—O3—Dy3	95.80 (19)	N7—Dy2—O13	86.2 (2)
Dy2—O4—Dy1	94.00 (18)				

**Table S3a.** *SHAPE* analysis of the Dy1(III) ion for complex **1**.

Label	Shape	Symmetry	Distortion(°)
EP-9	$D_{9h}$	Enneagon	31.153
OPY-9	$C_{8v}$	Octagonal pyramid	24.162
HBPY-9	$D_{7h}$	Heptagonal bipyramid	13.928
JTC-9	$C_{3v}$	Johnson triangular cupola J3	15.248
JCCU-9	$C_{4v}$	Capped cube J8	8.711
CCU-9	$C_{4v}$	Spherical-relaxed capped cube	7.629
JCSAPR-9	$C_{4v}$	Capped square antiprism J10	4.714
CSAPR-9	$C_{4v}$	Spherical capped square antiprism	3.954
JTCTPR-9	$D_{3h}$	Tricapped trigonal prism J51	4.993
TCTPR-9	$D_{3h}$	Spherical tricapped trigonal prism	4.692
JTDIC-9	$C_{3v}$	Tridiminished icosahedron J63	12.331
HH-9	$C_{2v}$	Hula-hoop	6.341
MFF-9	$C_s$	Muffin	2.701

**Table 3b.** *SHAPE* analysis of the Dy2(III) ion for complex **1**.

Label	Shape	Symmetry	Distortion(°)
OP-8	$D_{8h}$	Octagon	31.305
HPY-8	$C_{7v}$	Heptagonal pyramid	20.665
HBPY-8	$D_{6h}$	Hexagonal bipyramid	15.441
CU-8	$O_h$	Cube	11.397

SAPR-8	$D_{4d}$	Square antiprism	4.556
TDD-8	$D_{2d}$	Triangular dodecahedron	2.247
JGBF-8	$D_{2d}$	Johnson gyrobifastigium J26	14.506
JETBPY-8	$D_{3h}$	Johnson elongated triangular bipyramid J14	25.625
JBTPR-8	$C_{2v}$	Biaugmented trigonal prism J50	3.482
BTPR-8	$C_{2v}$	Biaugmented trigonal prism	2.592
JSD-8	$D_{2d}$	Snub diphenoïd J84	4.084
TT-8	$T_d$	Triakis tetrahedron	12.067
ETBPY-8	$D_{3h}$	Elongated trigonal bipyramid	21.643

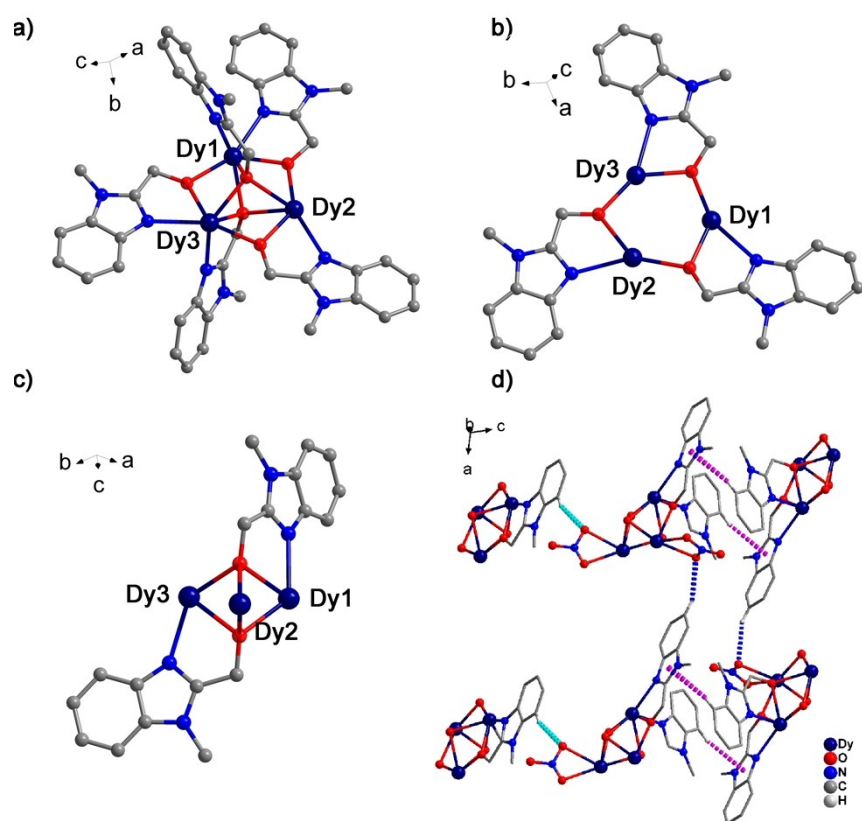
**Table 3c.** *SHAPE* analysis of the Dy3(III) ion for complex 1.

<b>Label</b>	<b>Shape</b>	<b>Symmetry</b>	<b>Distortion(°)</b>
OP-8	$D_{8h}$	Octagon	32.447
HPY-8	$C_{7v}$	Heptagonal pyramid	20.029
HBPY-8	$D_{6h}$	Hexagonal bipyramid	15.360
CU-8	$O_h$	Cube	11.341
SAPR-8	$D_{4d}$	Square antiprism	3.940
TDD-8	$D_{2d}$	Triangular dodecahedron	2.587
JGBF-8	$D_{2d}$	Johnson gyrobifastigium J26	14.557
JETBPY-8	$D_{3h}$	Johnson elongated triangular bipyramid J14	25.789
JBTPR-8	$C_{2v}$	Biaugmented trigonal prism J50	3.362
BTPR-8	$C_{2v}$	Biaugmented trigonal prism	2.680
JSD-8	$D_{2d}$	Snub diphenoïd J84	4.454

TT-8	$T_d$	Triakis tetrahedron	12.019
ETBPY-8	$D_{3h}$	Elongated trigonal bipyramid	21.6777

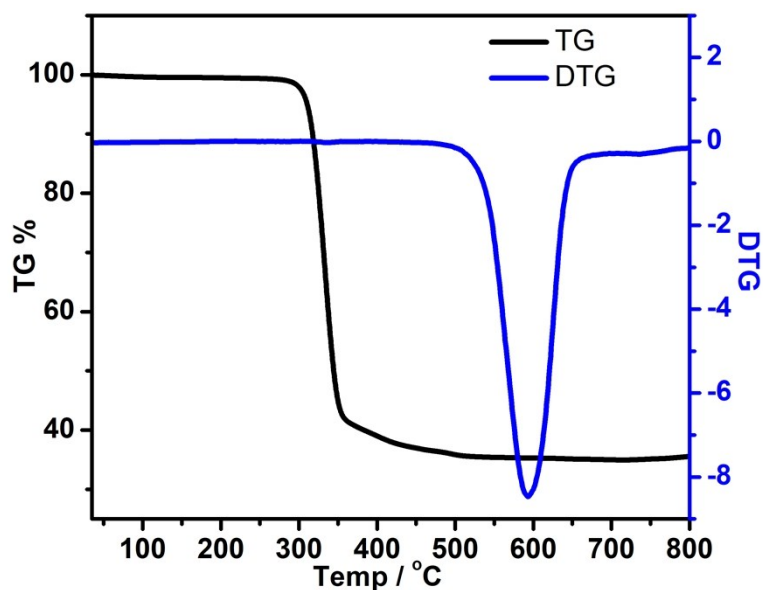
**Table S3d.** Ranges of bond lengths and angles for **1**.

Complex	<b>1</b>
Dy-N (Å)	2.419–2.522
Dy-O (ligand) (Å)	2.2.272–2.475
Dy-O (NO <sub>3</sub> <sup>-</sup> ) (Å)	2.435–2.500
Dy···Dy(Å)	3.537–3.593
Dy-O-Dy (°) (level)	100.800–103.795
Dy-O-Dy (°) (top and bottom)	93.934–95.860



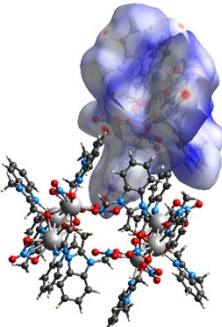
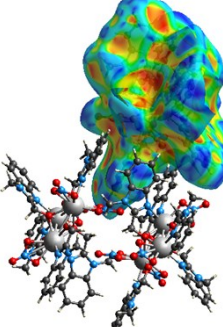
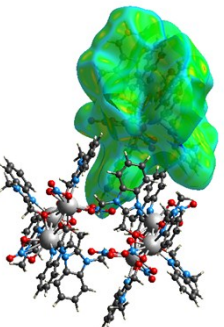
**Figure S1a.** (a) The structure after the coordination of nitrate was removed; (b) Only the structure located in the equatorial plane was retained; (c) The structure after the removal of the equatorial plane ligands. Coordinating NO<sub>3</sub><sup>-</sup> anions were omitted for clarity. (d) Structure of **1** showing the supramolecular interactions: C14–H14··· $\pi$  (PhC<sub>3</sub>N<sub>2</sub>) (pink dotted line), C22–H22···O15 hydrogen bond (blue dotted line) and C5–H5···O7 hydrogen bond (cyan dotted line) connecting clusters.

The thermal stability of the compounds was investigated at a heating rate of 5 °C/min over the temperature range from 35 to 800 °C in flowing N<sub>2</sub>. By integrating the thermogravimetric (TG) data (DTG), it could be clearly observed that the complex lost weight rapidly at around 300 °C, indicating the structural damage. Therefore, we could see from the TG curve that there was no solvent molecule between the molecules, and it was stable before 300 °C (Figure S1b).



**Figure S1b.** Thermogravimetry of **1** at a heating rate of 5 °C/min under N<sub>2</sub> atmosphere.

**Table S4.** Hirshfeld surfaces mapped with  $d_{norm}$  (left) showing Shape-index (middle) and Curvedness (right) for the **1**. Hirshfeld surface analysis were performed using CrystalExplorer (Version 3.1), S. K. Wolff, D. J. Grimwood, J. J. McKinnon, M. J. Turner, D. Jayatilaka, M. A. Spackman, University of Western Australia, 2012.

	$d_{norm}$	Shape Index	Curvedness
<b>1</b>			



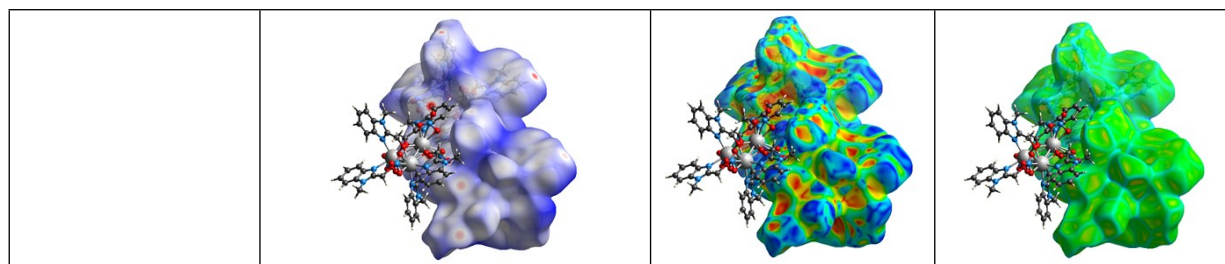


**Table S5.** Fingerprint plot for different interactions for **1** showing the percentage of contacts created to the total Hirshfeld surface area of the **1** molecules.  $d_i$  is the closest internal distance from a given point on the Hirshfeld surface;  $d_e$  is the closest external contact.

Inside + outside	<b>1</b>
All...All	
O...H	
N...H	

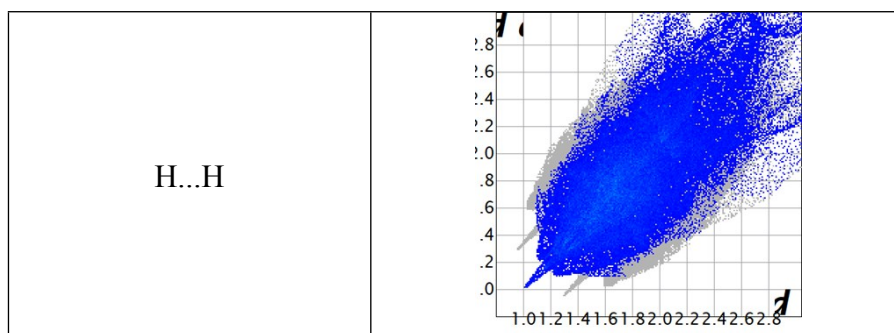


**Figure S2.** Temperature dependence of  $\chi_m T$  (a) Field dependence of the magnetization (b) for **1**.

**Table S6.** Selected parameters from the fitting result of the Cole-Cole plots for **1** under 0 Oe field.

Temp.(K)	<b>1</b>		
	$\tau$	$\alpha$	residual
4	2.53E-04	4.13E-01	2.72E+01
5	1.32E-02	3.41E-01	7.84E-02
6	1.14E-02	3.33E-01	7.17E-02
7	9.40E-03	3.24E-01	7.15E-02
8	7.41E-03	3.11E-01	8.55E-02
9	5.57E-03	2.93E-01	1.05E-01
10	3.99E-03	2.72E-01	1.20E-01
11	2.77E-03	2.51E-01	1.23E-01
12	1.88E-03	2.31E-01	1.12E-01
13	1.28E-03	2.16E-01	9.26E-02
14	8.58E-04	2.06E-01	6.84E-02
15	5.83E-04	2.00E-01	5.51E-02
16	3.95E-04	1.98E-01	4.19E-02
17	2.73E-04	2.02E-01	4.31E-02
18	1.90E-04	2.06E-01	4.08E-02
19	1.35E-04	2.07E-01	3.65E-02
20	9.70E-05	2.08E-01	3.25E-02
21	7.14E-05	2.07E-01	2.67E-02

**Table S7.** Magneto-structural data for triangular Dy<sub>3</sub> SMMs.

Cluster	$\Delta E$ (K)	Geometry [1]	Internal bridges	Ground state
[Dy <sub>3</sub> ( $\mu_3$ -OH) <sub>2</sub> L <sub>3</sub> Cl <sub>2</sub> (H <sub>2</sub> O) <sub>4</sub> ][Dy <sub>3</sub> ( $\mu_3$ -OH) <sub>2</sub> L <sub>3</sub> Cl(H <sub>2</sub> O) <sub>5</sub> ]Cl <sub>5</sub> ·19H <sub>2</sub> O <sup>a</sup>	17.4	[2]	$\mu_3$ -OH	AF
[Dy <sub>3</sub> ( $\mu_3$ -OH) <sub>2</sub> L <sub>3</sub> Cl(H <sub>2</sub> O) <sub>5</sub> ]Cl <sub>3</sub> ·4H <sub>2</sub> O·2MeOH·0.7MeCN <sup>a</sup>	29.8	[2]	$\mu_3$ -OH	AF
[Dy <sub>3</sub> ( $\mu_3$ OH) <sub>2</sub> (Hpovh) <sub>3</sub> (NO <sub>3</sub> ) <sub>3</sub> (MeOH) <sub>2</sub> (H <sub>2</sub> O)]NO <sub>3</sub> ·3CH <sub>3</sub> OH·2H <sub>2</sub> O <sup>b</sup>	26 2.9	CSAPR-9	$\mu_3$ -OH	AF
[Dy <sub>3</sub> ( $\mu_3$ OH) <sub>2</sub> (H <sub>2</sub> vovh) <sub>3</sub> Cl <sub>2</sub> (CH <sub>3</sub> OH)(H <sub>2</sub> O) <sub>3</sub> ][Dy <sub>3</sub> ( $\mu_3$ OH) <sub>2</sub> (H <sub>2</sub> vovh) <sub>3</sub> Cl <sub>2</sub> (H <sub>2</sub> O) <sub>4</sub> ]·Cl <sub>4</sub> ·2CH <sub>3</sub> OH·2CH <sub>3</sub> CN·7H <sub>2</sub> O <sup>b</sup>	10.5 [3] 39.7 [3]	[2]	$\mu_3$ -OH	AF
Dy <sub>3</sub> (HL)(H <sub>2</sub> L <sup>1</sup> )(NO <sub>3</sub> ) <sub>4</sub> <sup>c</sup>	42.6, 90.9 20.6	SAPR-8 CSAPR-9	$\mu_3$ -OR	AF
[Dy <sub>3</sub> (L <sup>2</sup> )( $\mu_3$ OH) <sub>2</sub> (NO <sub>3</sub> ) <sub>2</sub> (H <sub>2</sub> O) <sub>4</sub> ]·2NO <sub>3</sub> ·6MeOH·H <sub>2</sub> O <sup>d</sup>	-0.24	TDD-8	$\mu_3$ -OH	F
[Dy <sub>3</sub> (L <sup>2</sup> )( $\mu_3$ OH) <sub>2</sub> (SCN) <sub>4</sub> (H <sub>2</sub> O) <sub>2</sub> ]·3MeOH·2H <sub>2</sub> O <sup>d</sup>	7.7 [3]	TDD-8	$\mu_3$ -OH	F
[Dy <sub>3</sub> ( $\mu_3$ -OCH <sub>3</sub> ) <sub>2</sub> (HL <sup>3</sup> ) <sub>3</sub> (SCN)]·4CH <sub>3</sub> OH·2CH <sub>3</sub> CN·2H <sub>2</sub> O <sup>e</sup>	4.3 2.2	BTPR-8 TCTPR-9	$\mu_3$ -OCH <sub>3</sub>	U
[Dy <sub>3</sub> ( $\mu_3$ -N <sub>3</sub> )( $\mu_3$ -OH)(H <sub>2</sub> L <sup>3</sup> ) <sub>3</sub> (SCN) <sub>3</sub> ](SCN)·3CH <sub>3</sub> OH·H <sub>2</sub> O <sup>e</sup>	-1.4	TCTPR-9	$\mu_3$ -OH $\mu_3$ -N <sub>3</sub>	U
[Dy <sub>3</sub> ( $\mu$ -OH) <sub>2</sub> L <sub>3</sub> Cl(H <sub>2</sub> O) <sub>5</sub> ]Cl <sub>3</sub> ·4H <sub>2</sub> O·2MeOH·0.7MeCN <sup>f</sup>	13	TDD-8	$\mu_3$ -OR	F
[Dy <sub>3</sub> L <sup>R</sup> (NO <sub>3</sub> ) <sub>3</sub> (OH) <sub>2</sub> ]·NO <sub>3</sub> <sup>g</sup>		JBTPR-8	$\mu_3$ -OH	F
[Dy <sub>3</sub> L <sup>S</sup> (NO <sub>3</sub> ) <sub>3</sub> (OH) <sub>2</sub> ]·NO <sub>3</sub> <sup>g</sup>		JBTPR-8	$\mu_3$ -OH	F
Dy <sub>3</sub> ·[BPh <sub>4</sub> ] <sup>h</sup>	24.1 [4] 13.6 [4]	BTPR-8	$\mu_3$ -OCH <sub>3</sub>	AF
Dy <sub>3</sub> ·[Dy(NO <sub>3</sub> ) <sub>6</sub> ] <sup>h</sup>	13.6 [4]	BTPR-8	$\mu_3$ -OCH <sub>3</sub>	AF
[Dy <sub>3</sub> L <sub>R</sub> ( $\mu_3$ -OH) <sub>2</sub> (H <sub>2</sub> O) <sub>2</sub> (SCN) <sub>4</sub> ]·6CH <sub>3</sub> OH <sup>i</sup>	37	TDD-8	$\mu_3$ -OH	AF
Dy <sub>3</sub> L <sub>5</sub> (NO <sub>3</sub> ) <sub>4</sub> <sup>j</sup>	130	MFF-9 TDD-8	$\mu_3$ -OH	AF

[1] All geometries are distorted. CSAPR-9=capped square antiprism; SAPR-8=square antiprism; TDD-8=trigonal dodecahedron; BTPR-8=bicapped trigonalprism; TCTPR-9=tricapped trigonal prism;JBTPR-8=Biaugmented trigonal prism J50; MFF-9=Muffin; AF=antiferromagnetic coupling; F=ferromagnetic coupling; U=unknown; [2] Pentagonal bipyramid in which one site in the pentagonal plane has been replaced by two  $\mu$ -hydroxo sites above and below it. HL=*o*-vanillin;H<sub>2</sub>povh=*N*-(pyridylmethylene)-*o*-vanilloylhydrazone; H<sub>2</sub>vovh=*N*-vanillidene-*O*-vanilloylhydrazone; H<sub>4</sub>L<sup>1</sup>=*N,N,N,N*-tetrakis(2-hydroxyethyl)ethylenediamine;H<sub>3</sub>L<sup>2</sup>=trinucleatingnonadentate N<sub>6</sub>O<sub>3</sub> ligand; H<sub>3</sub>L<sup>3</sup>=2,6-diformyl-4-methylphenoldi(benzoylhydrazone); [3] With a dc applied field of 500 Oe; [4] With a dc appliedfield of 1000 Oe.

(a) J. Tang, I. Hewitt, N. T. Madhu, G. Chastanet, W. Wernsdorfer, C. E. Anson, C. Benelli, R. Sessoli, A. K. Powell, *Angew. Chem. Int. Ed.* **2006**, *45*, 1729;

(b) S. Xue, X. H. Chen, L. Zhao, Y. N. Guo, J. Tang, *Inorg. Chem.* **2012**, *51*, 13264;

(c) Y. X. Wang, W. Shi, H. Li, Y. Song, L. Fang, Y. Lan, A. K. Powell, W. Wernsdorfer, L. Ungur, L. F. Chibotaru, M. Shen, P. Cheng, *Chem. Sci.* **2012**, *3*, 3366;

(d) S. Y. Lin, Y. N. Guo, Y. Guo, L. Zhao, P. Zhang, H. Ke, J. Tang, *Chem. Commun.* **2012**, *48*, 6924;

(e) S. Y. Lin, L. Zhao, Y. N. Guo, P. Zhang, Y. Guo, J. Tang, *Inorg. Chem.* **2012**, *51*, 10522;

(f) S. Shen, S. Xue, S.-Y. Lin, L. Zhao, J. Tang, *Dalton Trans.*, **2013**, *42*, 10413;

(g) M. J. Kobyłka, K. Ślepokura, M. A. Rodicio, M. Paluch, J. Lisowski, *Inorg. Chem.* **2013**, *52*, 12893;

(h) M. M. Hänninen, A. J. Mota, D. Aravena, E. Ruiz, R. Sillanpää, A. Camón, M. Evangelisti, E. Colacio, *Chem. Eur. J.* **2014**, *20*, 8410;

(i) S.-Y. Lin, C. Wang, L. Zhao, J. Tang, *Chem. Asian J.* **2014**, *9*, 3558;

(j) *this work*.

## Computational details

Complex **1** has three types of Dy<sup>III</sup> fragments, and thus we need to calculate three Dy<sup>III</sup> fragments. Complete-active-space self-consistent field (CASSCF) calculations on individual Dy<sup>III</sup> fragments of the model structures (see Figure S1 for the calculated model structure of **1(Dy1)**) extracted from the compound on the basis of single-crystal X-ray determined geometry have been carried out with MOLCAS 8.2 program package.<sup>S1</sup> For complex **1**, each Dy<sup>III</sup> fragment was calculated keeping the experimentally determined structure of the corresponding compound while replacing the neighboring Dy<sup>III</sup> ions by diamagnetic Lu<sup>III</sup>.

The basis sets for all atoms are atomic natural orbitals from the MOLCAS ANO-RCC library: ANO-RCC-VTZP for Dy<sup>III</sup> ion; VTZ for close O and N; VDZ for distant atoms. The calculations employed the second order Douglas-Kroll-Hess Hamiltonian, where scalar relativistic contractions were taken into account in the basis set and the spin-orbit couplings were handled separately in the restricted active space state interaction (RASSI-SO) procedure. For individual Dy<sup>III</sup> fragment, active electrons in 7 active spaces include all *f* electrons (CAS(9 in 7)) in the CASSCF calculation. To exclude all the doubts, we calculated all the roots in the active space. We have mixed the maximum number of spin-free state which was possible with our hardware (all from 21 sextets, 128 from 224 quadruplets, 130 from 490 doublets). Single–Aniso<sup>S2</sup> program was used to obtain energy levels, *g* tensors, *m<sub>J</sub>* values, magnetic axes, *et al.*, based on the above CASSCF/RASSI calculations.

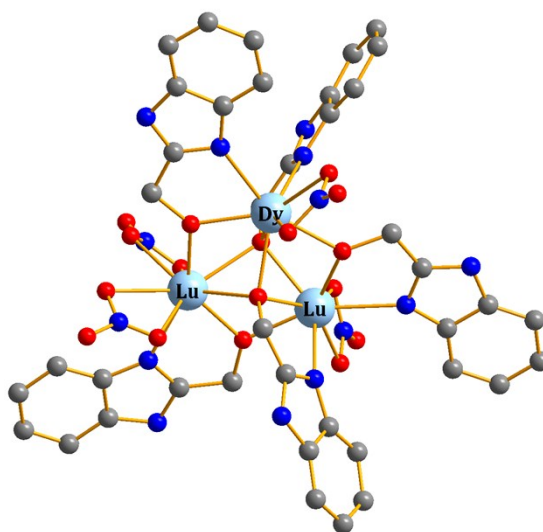


**Figure S3.** Calculated model structure of Dy<sup>III</sup> fragment of **1(Dy1)** of complex **1**; H atoms are omitted.

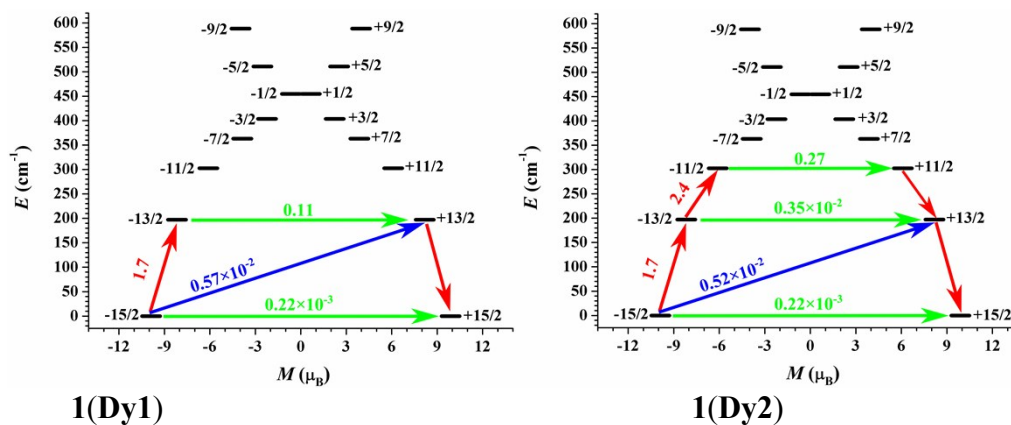
**Table S8.** Calculated energy levels (cm<sup>-1</sup>), *g*(*g<sub>x</sub>*, *g<sub>y</sub>*, *g<sub>z</sub>*) tensors and *m<sub>J</sub>* values of the lowest eight Kramers doublets (KDs) of individual Dy<sup>III</sup> fragments of **1(Dy1)**, **1(Dy2)** and **1(Dy3)** of complex **1** using CASSCF/RASSI with MOLCAS 8.2.

KDs	<b>1(Dy1)</b>			<b>1(Dy2)</b>			<b>1(Dy3)</b>		
	<i>E/cm<sub>1</sub><sup>-1</sup></i>	<i>g</i>	<i>m<sub>J</sub></i>	<i>E/cm<sub>1</sub><sup>-1</sup></i>	<i>g</i>	<i>m<sub>J</sub></i>	<i>E/cm<sub>1</sub><sup>-1</sup></i>	<i>g</i>	<i>m<sub>J</sub></i>
1	0.0	0.000	±15/2	0.0	0.003	±15/2	0.0	0.002	±15/2

		0.001 19.765			0.005 19.809			0.002 19.790	
2	197.2	0.279 0.389 16.604	$\pm 13/2$	174.7	0.090 0.116 17.017	$\pm 13/2$	224.8	0.102 0.133 16.770	$\pm 13/2$
3	302.6	1.454 1.929 12.556	$\pm 11/2$	303.5	0.590 0.950 13.907	$\pm 11/2$	355.3	0.575 0.616 13.321	$\pm 11/2$
4	363.0	2.718 4.775 8.657	$\pm 7/2$	406.1	2.930 3.487 10.410	$\pm 9/2$	432.7	1.200 2.021 8.991	$\pm 9/2$
5	403.6	2.763 3.343 12.050	$\pm 3/2$	483.2	8.830 7.522 0.946	$\pm 5/2$	461.0	2.853 6.674 11.520	$\pm 3/2$
6	454.7	0.783 1.621 15.198	$\pm 1/2$	521.3	2.473 4.564 12.461	$\pm 3/2$	510.4	0.291 0.897 17.337	$\pm 1/2$
7	510.7	0.042 0.126 18.569	$\pm 5/2$	585.2	0.816 1.674 15.714	$\pm 1/2$	538.2	0.037 0.299 18.268	$\pm 7/2$
8	588.1	0.008 0.029 19.641	$\pm 9/2$	698.7	0.062 0.159 18.634	$\pm 7/2$	580.7	0.070 0.193 18.666	$\pm 5/2$

**Table S9.** Wave functions with definite projection of the total moment  $|m_J\rangle$  for the lowest three Kramers doublets (KDs) of individual Dy<sup>III</sup> fragments of **1(Dy1)**, **1(Dy2)** and **1(Dy3)** for complex **1** using CASSCF/RASSI with MOLCAS 8.2.

	$E/\text{cm}^{-1}$	wave functions
<b>1(Dy1)</b>	0.0	99% $ \pm 15/2\rangle$
	197.2	89% $ \pm 13/2\rangle$ +6% $ \pm 9/2\rangle$
	302.6	4% $ \pm 13/2\rangle$ +64% $ \pm 11/2\rangle$ +20% $ \pm 7/2\rangle$ +5% $ \pm 1/2\rangle$
<b>1(Dy2)</b>	0.0	99% $ \pm 15/2\rangle$
	174.7	92% $ \pm 13/2\rangle$ +4% $ \pm 9/2\rangle$
	303.5	4% $ \pm 13/2\rangle$ +75% $ \pm 11/2\rangle$ +12% $ \pm 9/2\rangle$ +7% $ \pm 7/2\rangle$
<b>1(Dy3)</b>	0.0	99% $ \pm 15/2\rangle$
	224.8	88% $ \pm 13/2\rangle$ +6% $ \pm 9/2\rangle$
	355.3	6% $ \pm 13/2\rangle$ +64% $ \pm 11/2\rangle$ +5% $ \pm 9/2\rangle$ +15% $ \pm 7/2\rangle$



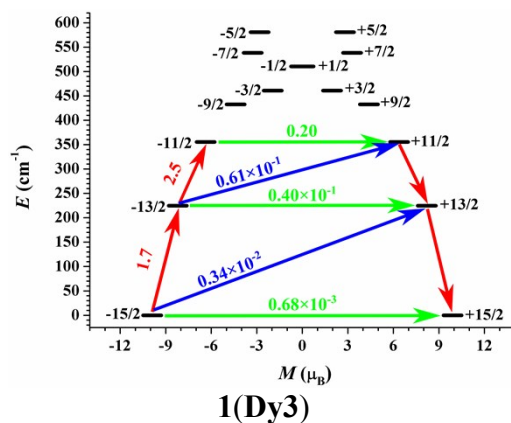


**Figure S4.** Magnetization blocking barriers for individual Dy<sup>III</sup> fragments of **1(Dy1)**, **1(Dy2)** and **1(Dy3)** in complex **1**. The thick black lines represent the Kramer's doublets as a function of their magnetic moment along the magnetic axis. The green lines correspond to diagonal quantum tunneling of magnetization (QTM); the blue line represent off-diagonal relaxation process. The numbers at each arrow stand for the mean absolute value of the corresponding matrix element of transition magnetic moment.

To fit the exchange interactions in complex **1**, we took two steps to obtain them. Firstly, we calculated individual Dy<sup>III</sup> fragments using CASSCF to obtain the corresponding magnetic properties. Then, the exchange interaction between the magnetic centers is considered within the Lines model,<sup>S3</sup> while the account of the dipole-dipole magnetic coupling is treated exactly. The Lines model is effective and has been successfully used widely in the research field of *f*-element single-molecule magnets.<sup>S4</sup>

For complex **1**, there are three types of *J*.

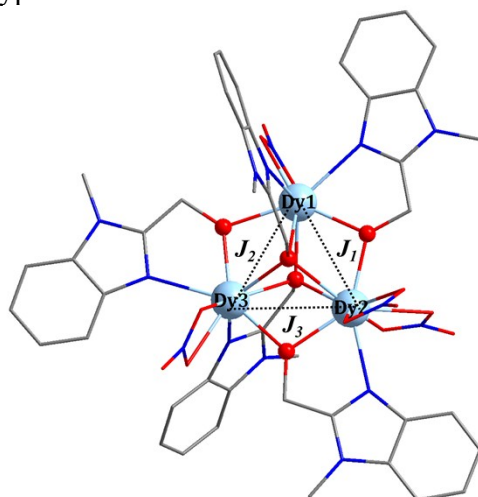


**Figure S5.** Three types of  $J_1$ ,  $J_2$  and  $J_3$  in complex **1**.

The exchange Ising Hamiltonian is:

$$\hat{H}_{exch} = -J_1 \hat{S}_{By1}^z \hat{S}_{By2}^z - J_2 \hat{S}_{By1}^z \hat{S}_{By3}^z - J_3 \hat{S}_{By2}^z \hat{S}_{By3}^z \quad (S1)$$

The  $J_{total}$  is the parameter of the total magnetic interaction ( $J_{total} = J_{dipolar} + J_{exchange}$ ) between magnetic center ions. The  $S_{By}^z = \pm 1/2$  are the ground pseudospin on the Dy<sup>III</sup> sites. The dipolar magnetic coupling can be calculated exactly, while the exchange coupling constants were fitted through

comparison of the computed and measured magnetic susceptibilities using the Poly\_Aniso program.<sup>S2</sup>

**Table S10.** Exchange energies ( $\text{cm}^{-1}$ ) and main values of the  $g_z$  for the lowest four exchange doublets of complex **1**.

	<b>1</b>	
	$E/\text{cm}^{-1}$	$g_z$
1	0.0	19.781
2	3.1	33.938
3	3.5	52.535
4	4.6	19.780

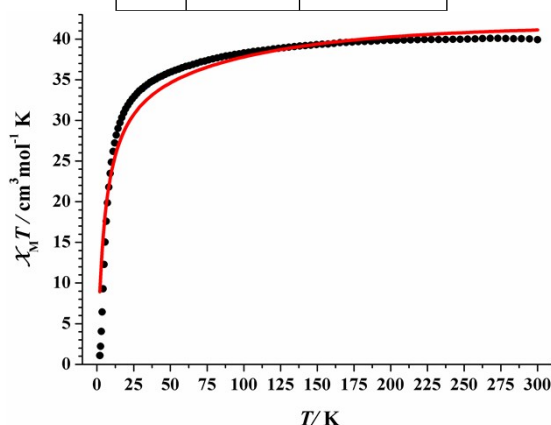


**Figure S6.** Calculated (red solid line) and experimental (black circle dot) data of magnetic susceptibility of complex **1**. The intermolecular interactions  $zJ'$  of complex **1** was fitted to  $-0.30\text{cm}^{-1}$ .

### References:

- S1 (a) Aquilante, F.; De Vico, L.; Ferré, N.; Ghigo, G.; Malmqvist, P.-Å.; Neogrady, P.; Pedersen, T. B.; Pitonak, M.; Reiher, M.; Roos, B. O.; Serrano-Andrés, L.; Urban, M.; Veryazov, V.; Lindh, R. *J. Comput. Chem.*, **2010**, *31*, 224. (b) Veryazov, V.; Widmark, P. -O.; Serrano-Andres, L.; Lindh, R.; Roos, B. O. *Int. J. Quantum Chem.*, **2004**, *100*, 626. (c) Karlström, G.; Lindh, R.; Malmqvist, P. -Å.; Roos, B. O.; Ryde, U.; Veryazov, V.; Widmark, P. -O.; Cossi, M.; Schimmelpfennig, B.; Neogrady, P.; Seijo, L. *Comput. Mater. Sci.*, **2003**, *28*, 222.
- S2 (a) Chibotaru, L. F.; Ungur, L.; Soncini, A. *Angew. Chem. Int. Ed.*, **2008**, *47*, 4126. (b) Ungur, L.; Van den Heuvel, W.; Chibotaru, L. F. *New J. Chem.*, **2009**, *33*, 1224. (c) Chibotaru, L. F.; Ungur, L.; Aronica, C.; Elmoll, H.; Pilet, G.; Luneau, D. *J. Am. Chem. Soc.*, **2008**, *130*, 12445.
- S3 Lines, M. E. *J. Chem. Phys.* **1971**, *55*, 2977.
- S4 (a) Mondal, K. C.; Sundt, A.; Lan, Y. H.; Kostakis, G. E.; Waldmann, O.; Ungur, L.; Chibotaru, L. F.; Anson, C. E.; Powell, A. K. *Angew. Chem. Int. Ed.* **2012**, *51*, 7550. (b) Langley, S. K.; Wielechowski, D. P.; Vieru, V.; Chilton, N. F.; Moubaraki, B.; Abrahams, B. F.; Chibotaru, L. F.; Murray, K. S. *Angew. Chem. Int. Ed.* **2013**, *52*, 12014.



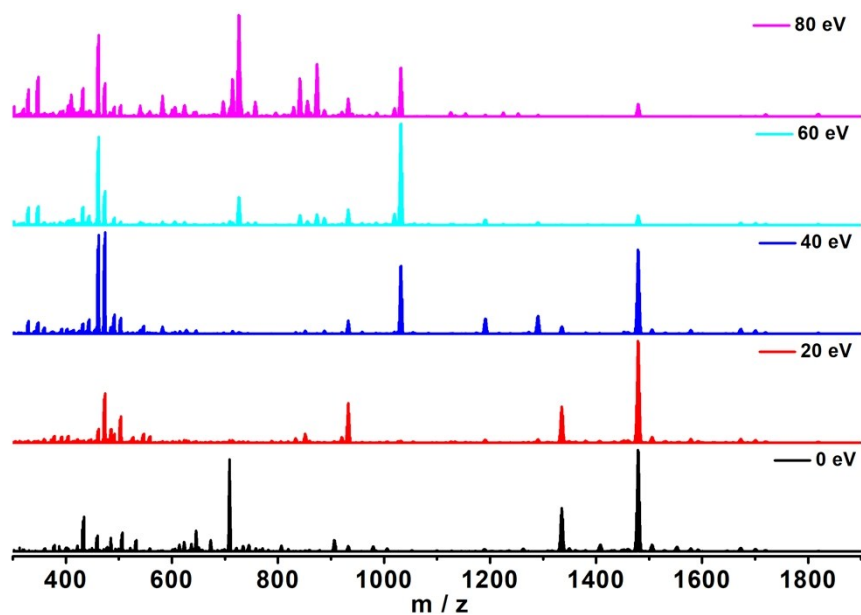


**Figure S7.** Positive ESI-MS spectra of **1** in DMF (In-Source CID 0, 20, 40, 60, 80 eV).

**Table S11.** Major species assigned in the ESI-MS of **1** in positive mode.

<b>1</b> (In-Source CID 0 eV)			
Peaks	Relative Intensity	Obs. <i>m/z</i>	Calc. <i>m/z</i>
$[\text{Dy}(\text{L})(\text{NO}_3)(\text{CH}_3\text{OH})(\text{H}_2\text{O})\text{-3H}]^+$	0.338	434.01	434.00
$[\text{Dy}_3(\text{L})_5(\text{NO}_3)_2]^{2+}$	0.896	708.56	708.56
$[\text{Dy}_3(\text{L})_4(\text{NO}_3)_3(\text{OH})]^+$	0.420	1335.03	1335.02
$[\text{Dy}_3(\text{L})_5(\text{NO}_3)_3]^+$	1	1479.11	1479.10
<b>1</b> (In-Source CID 20 eV)			
$[\text{Dy}(\text{L})(\text{NO}_3)(\text{CH}_3\text{O})(\text{CH}_3\text{OH})(\text{DMF})+\text{H}]^+$	0.135	462.07	462.10
$[\text{Dy}(\text{L})(\text{OH})(\text{CH}_3\text{CN})(\text{DMF})(\text{H}_2\text{O})]^+$	0.486	474.07	474.09
$[\text{Dy}_2(\text{L})_3(\text{NO}_3)_2]^+$	0.379	932.05	932.05
$[\text{Dy}_3(\text{L})_4(\text{NO}_3)_3(\text{OH})]^+$	0.348	1335.03	1335.02
$[\text{Dy}_3(\text{L})_5(\text{NO}_3)_3]^+$	1	1479.11	1479.10
<b>1</b> (In-Source CID 40 eV)			
$[\text{Dy}(\text{L})(\text{NO}_3)(\text{CH}_3\text{O})(\text{CH}_3\text{OH})(\text{DMF})+\text{H}]^+$	0.966	462.07	462.10
$[\text{Dy}(\text{L})(\text{OH})(\text{CH}_3\text{CN})(\text{DMF})(\text{H}_2\text{O})]^+$	1	474.07	474.09



$[\text{Dy}_2(\text{L})_3(\text{NO}_3)_2]^+$	0.131	932.05	932.05
$[\text{Dy}_2(\text{L})_3(\text{NO}_3)_2(\text{CH}_3\text{CN})_2(\text{H}_2\text{O})]^+$	0.705	1032.13	1032.10
$[\text{Dy}_3(\text{L})_4(\text{NO}_3)_3(\text{OH})]^+$	0.072	1335.03	1335.02
$[\text{Dy}_3(\text{L})_5(\text{NO}_3)_3]^+$	0.823	1479.12	1479.10
<b>1 (In-Source CID 60 eV)</b>			
$[\text{Dy}(\text{L})(\text{NO}_3)(\text{CH}_3\text{O})(\text{CH}_3\text{OH})(\text{DMF})+\text{H}]^+$	0.810	462.07	462.10
$[\text{Dy}(\text{L})(\text{OH})(\text{CH}_3\text{CN})(\text{DMF})(\text{H}_2\text{O})]^+$	0.314	474.07	474.09
$[\text{Dy}_2(\text{L})_2(\text{NO}_3)(\text{OH})]^+$	0.258	726.00	725.99
$[\text{Dy}_2(\text{L})_3(\text{NO}_3)_2]^+$	0.144	932.05	932.05
$[\text{Dy}_2(\text{L})_3(\text{NO}_3)_2(\text{CH}_3\text{CN})_2(\text{H}_2\text{O})]^+$	1	1032.13	1032.10
$[\text{Dy}_3(\text{L})_5(\text{NO}_3)_3]^+$	0.090	1479.12	1479.10
<b>1 (In-Source CID 80 eV)</b>			
$[\text{Dy}(\text{L})(\text{NO}_3)(\text{CH}_3\text{O})(\text{CH}_3\text{OH})(\text{DMF})+\text{H}]^+$	0.800	462.07	462.10
$[\text{Dy}(\text{L})(\text{OH})(\text{CH}_3\text{CN})(\text{DMF})(\text{H}_2\text{O})]^+$	0.324	474.07	474.09
$[\text{Dy}_2(\text{L})_2(\text{NO}_3)(\text{OH})]^+$	1	726.00	725.99
$[\text{Dy}_2(\text{L})_3(\text{NO}_3)_2]^+$	0.175	932.05	932.05
$[\text{Dy}_2(\text{L})_3(\text{NO}_3)_2(\text{CH}_3\text{CN})_2(\text{H}_2\text{O})]^+$	0.480	1032.12	1032.10
$[\text{Dy}_3(\text{L})_5(\text{NO}_3)_3]^+$	0.121	1479.11	1479.10

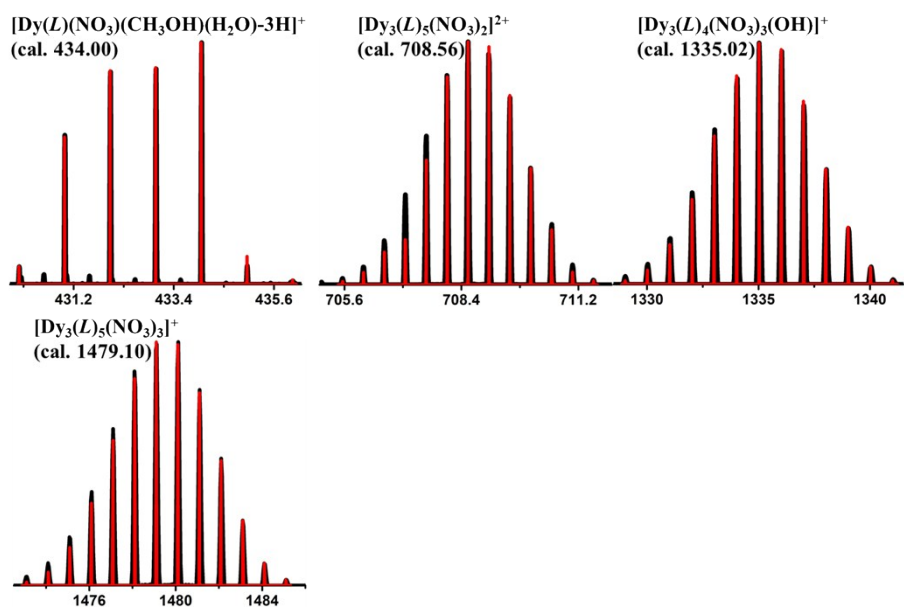


**Figure S8.** The superposed simulated and observed spectra of several species for **1** (In-Source CID 0 eV).

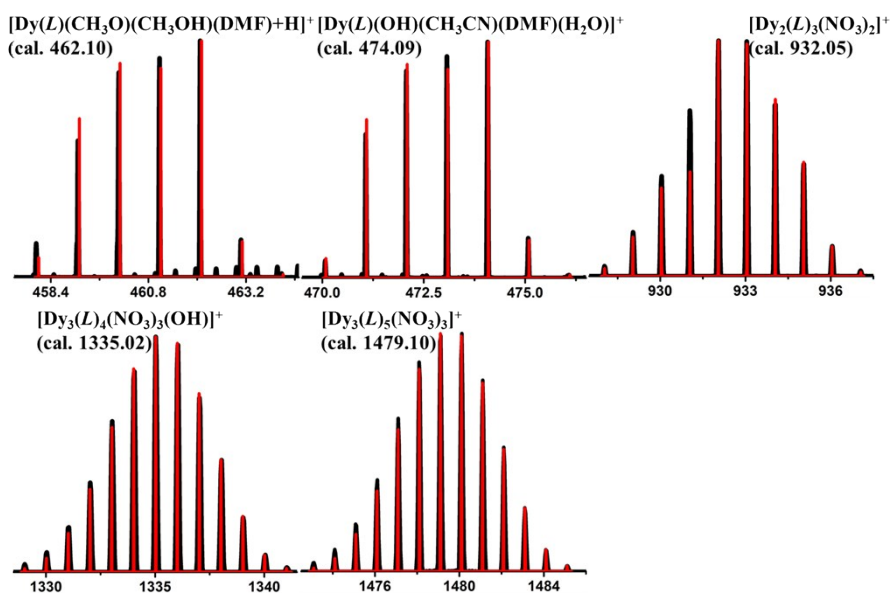


**Figure S9.** The superposed simulated and observed spectra of several species for **1** (In-Source CID 20 eV).

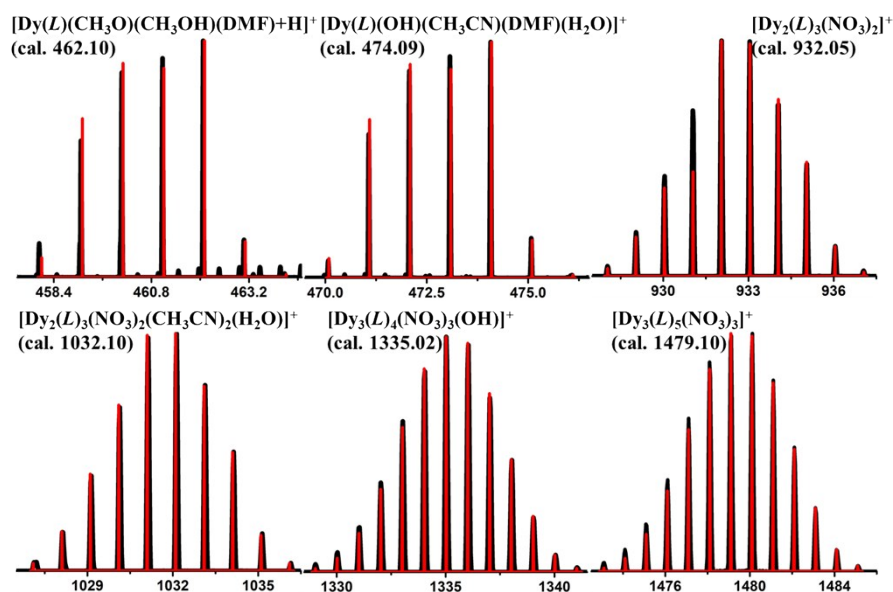


**Figure S10.** The superposed simulated and observed spectra of several species for **1** (In-Source CID 40, 60 and 80 eV).

#### Negative mode ESI-MS:

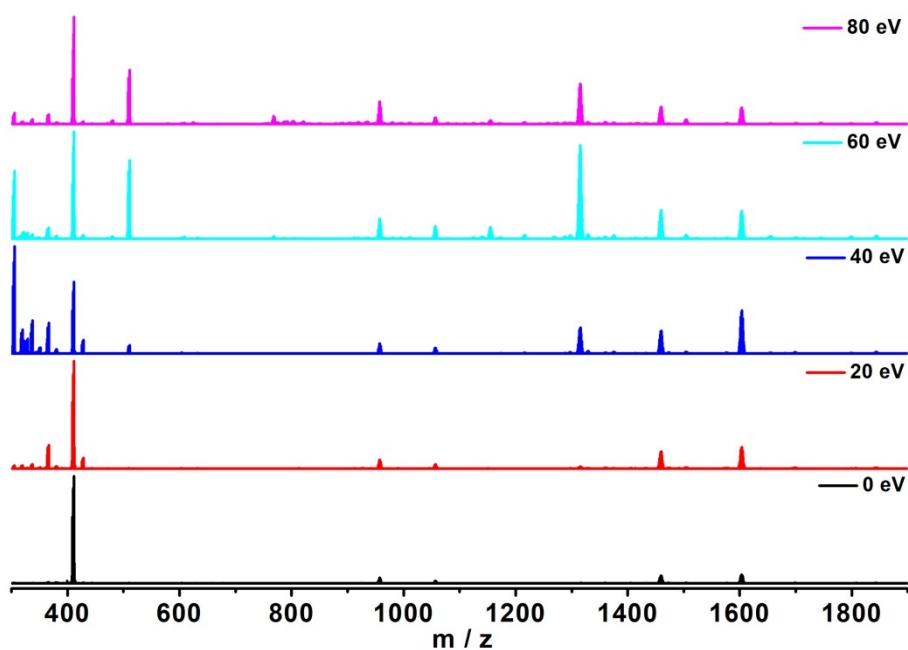


**Figure S11.** Negative ESI-MS spectra of **1** in DMF (In-Source CID 0, 20, 40, 60, 80 eV).

**Table S12.** Major species assigned in the ESI-MS of **1** in negative mode.

<b>1</b> (In-Source CID 0 eV)			
Peaks	Relative Intensity	Obs. <i>m/z</i>	Calc. <i>m/z</i>
[Dy(NO <sub>3</sub> ) <sub>4</sub> ] <sup>-</sup>	1	411.88	411.88

$[\text{Dy}_2(\text{L})_2(\text{NO}_3)_5]^-$	0.052	956.93	956.94
$[\text{Dy}_2(\text{L})_3(\text{NO}_3)_4]^-$	0.022	1056.02	1056.02
$[\text{Dy}_3(\text{L})_4(\text{NO}_3)_5(\text{OH})]^-$	0.070	1459.00	1459.00
$[\text{Dy}_3(\text{L})_5(\text{NO}_3)_5]^-$	0.081	1603.06	1603.08
<b>1 (In-Source CID 20 eV)</b>			
$[\text{Dy}(\text{NO}_3)_3(\text{OH})]^-$	0.219	366.90	366.90
$[\text{Dy}(\text{NO}_3)_4]^-$	1	411.88	411.88
$[\text{Dy}_2(\text{L})_2(\text{NO}_3)_5]^-$	0.082	956.95	956.94
$[\text{Dy}_2(\text{L})_3(\text{NO}_3)_4]^-$	0.039	1056.03	1056.02
$[\text{Dy}_3(\text{L})_3(\text{NO}_3)_5(\text{OH})_2]^-$	0.017	1314.92	1314.90
$[\text{Dy}_3(\text{L})_4(\text{NO}_3)_5(\text{OH})]^-$	0.156	1459.00	1459.00
$[\text{Dy}_3(\text{L})_5(\text{NO}_3)_5]^-$	0.195	1603.06	1603.08
<b>1 (In-Source CID 40 eV)</b>			
$[\text{Dy}(\text{NO}_3)_3(\text{OH})]^-$	0.288	366.90	366.90
$[\text{Dy}(\text{NO}_3)_4]^-$	1	411.88	411.88
$[\text{Dy}(\text{NO}_3)_4(\text{H}_2\text{O})]^-$	0.126	428.88	428.88
$[\text{Dy}(\text{NO}_3)_4(\text{CH}_3\text{CN})(\text{H}_2\text{O})]^-$	0.079	510.97	510.94
$[\text{Dy}_2(\text{L})_2(\text{NO}_3)_5]^-$	0.095	956.95	956.94
$[\text{Dy}_2(\text{L})_3(\text{NO}_3)_4]^-$	0.053	1056.03	1056.02
$[\text{Dy}_3(\text{L})_3(\text{NO}_3)_5(\text{OH})_2]^-$	0.241	1314.93	1314.90
$[\text{Dy}_3(\text{L})_4(\text{NO}_3)_5(\text{OH})]^-$	0.210	1459.00	1459.00
$[\text{Dy}_3(\text{L})_5(\text{NO}_3)_5]^-$	0.392	1603.06	1603.08
<b>1 (In-Source CID 60 eV)</b>			
$[\text{Dy}(\text{NO}_3)_3(\text{OH})]^-$	0.106	366.90	366.90
$[\text{Dy}(\text{NO}_3)_4]^-$	1	411.88	411.88
$[\text{Dy}(\text{NO}_3)_4(\text{H}_2\text{O})]^-$	0.033	428.88	428.88

$[\text{Dy}(\text{NO}_3)_4(\text{CH}_3\text{CN})(\text{H}_2\text{O})]^-$	0.732	510.97	510.94
$[\text{Dy}_2(\text{L})_2(\text{NO}_3)_5]^-$	0.188	956.97	956.94
$[\text{Dy}_2(\text{L})_3(\text{NO}_3)_4]^-$	0.111	1056.03	1056.02
$[\text{Dy}_3(\text{L})_3(\text{NO}_3)_5(\text{OH})_2]^-$	0.872	1314.93	1314.90
$[\text{Dy}_3(\text{L})_4(\text{NO}_3)_5(\text{OH})]^-$	0.262	1459.00	1459.00
$[\text{Dy}_3(\text{L})_5(\text{NO}_3)_5]^-$	0.256	1603.06	1603.08
<b>1</b> (In-Source CID 80 eV)			
$[\text{Dy}(\text{NO}_3)_3(\text{OH})]^-$	0.090	366.90	366.90
$[\text{Dy}(\text{NO}_3)_4]^-$	1	411.88	411.88
$[\text{Dy}(\text{NO}_3)_4(\text{CH}_3\text{CN})(\text{H}_2\text{O})]^-$	0.504	510.97	510.94
$[\text{Dy}_2(\text{L})_2(\text{NO}_3)_5]^-$	0.209	956.93	956.94
$[\text{Dy}_2(\text{L})_3(\text{NO}_3)_4]^-$	0.059	1056.03	1056.02
$[\text{Dy}_3(\text{L})_3(\text{NO}_3)_5(\text{OH})_2]^-$	0.376	1314.93	1314.90
$[\text{Dy}_3(\text{L})_4(\text{NO}_3)_5(\text{OH})]^-$	0.157	1459.00	1459.00
$[\text{Dy}_3(\text{L})_5(\text{NO}_3)_5]^-$	0.151	1603.06	1603.08

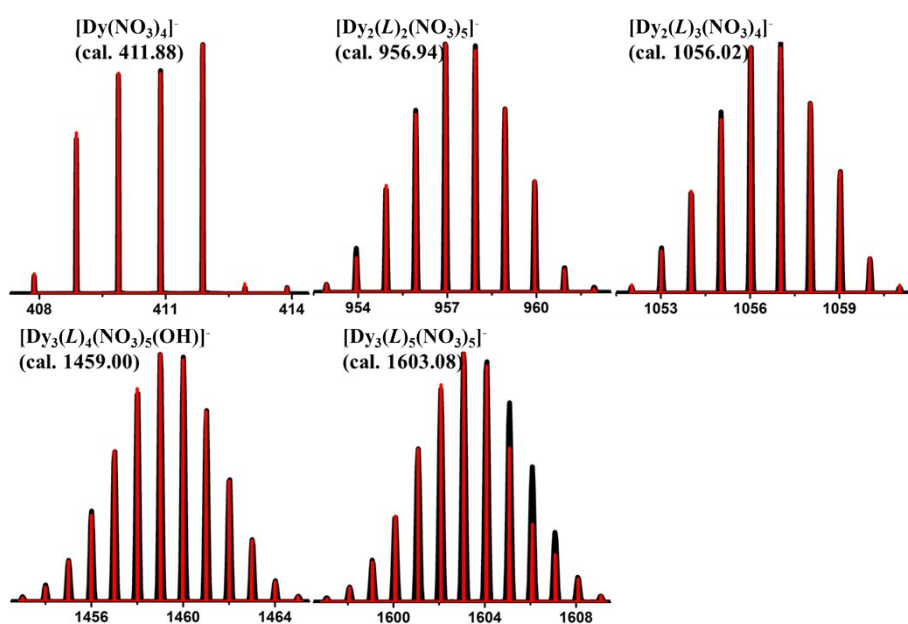


**Figure S12.** The superposed simulated and observed spectra of several species for **1** (In-Source CID 0 eV).

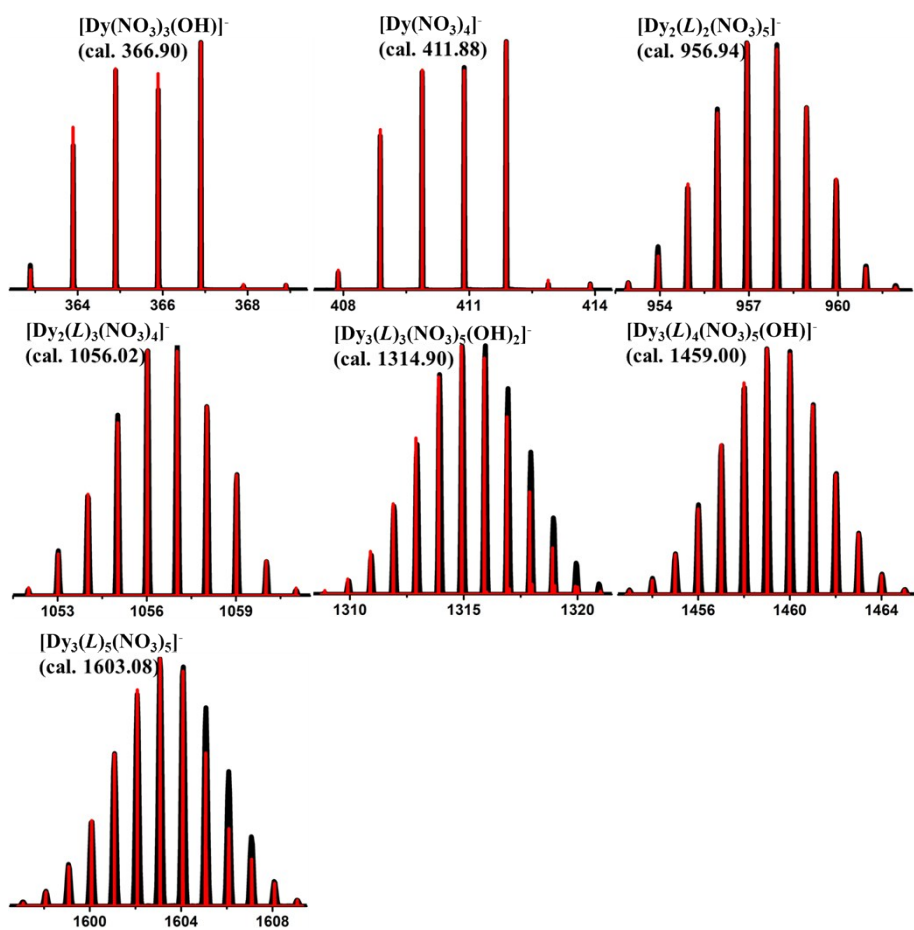


**Figure S13.** The superposed simulated and observed spectra of several species for **1** (In-Source CID 20 eV).

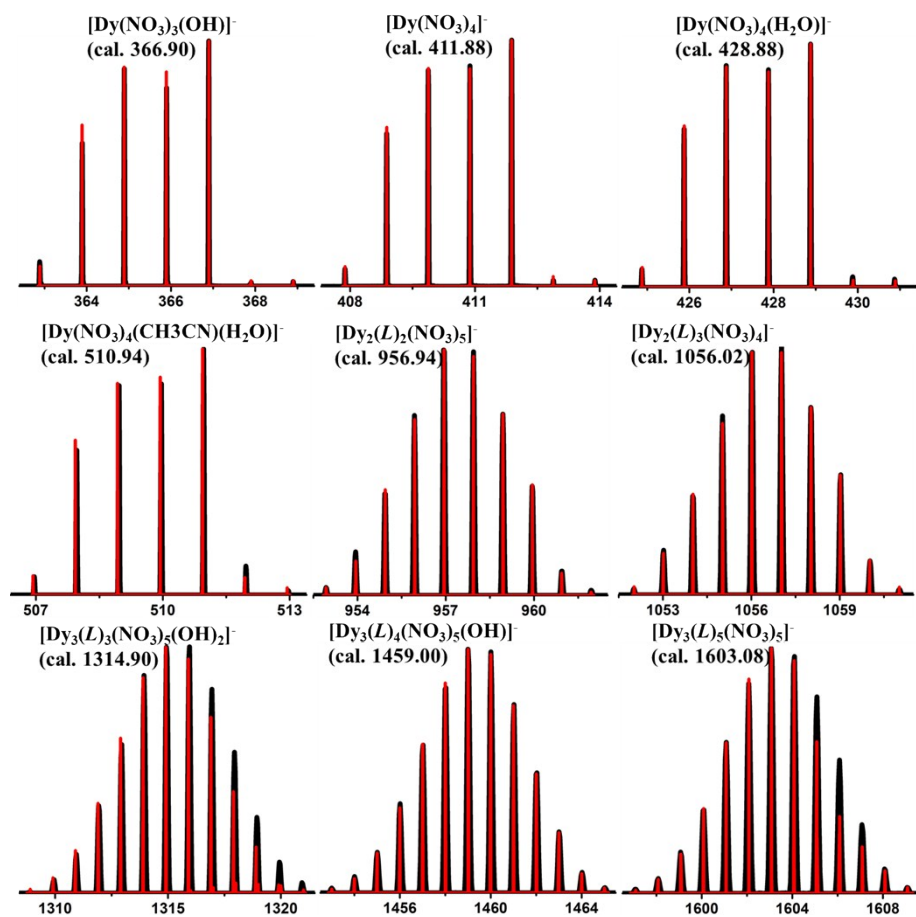


**Figure S14.** The superposed simulated and observed spectra of several species for **1** (In-Source CID 40, 60 and 80 eV).

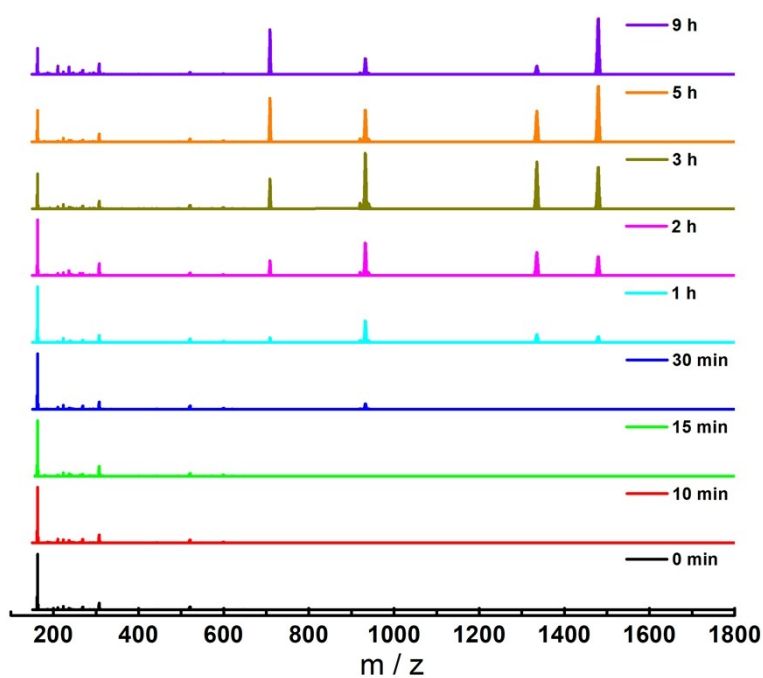


**Figure S15.** ESI-MS at different times during the reaction from *HL* and  $\text{Dy}(\text{NO}_3)_3 \cdot 6\text{H}_2\text{O}$  under ambient conditions.

**Table S13.** Major species assigned in the Time-dependent ESI-MS of **1** in positive mode.

m/z	Fragment	Relative Intensity						
		0min	30min	1 h	2 h	3 h	5 h	9 h
163.08	[HL] <sup>+</sup> (cal. 163.09)	1	1	1	1	0.626	0.569	0.469
521.95	[KDy(L)(NO <sub>3</sub> ) <sub>2</sub> (H <sub>2</sub> O) <sub>2</sub> ] <sup>+</sup> (cal. 921.95)	0.055	0.062	0.065	0.046	0.064	0.054	0.039
708.56	[Dy <sub>3</sub> (L) <sub>5</sub> (NO <sub>3</sub> ) <sub>2</sub> ] <sup>2+</sup> (cal. 708.56)			0.090	0.269	0.537	0.785	0.804
932.05	[Dy <sub>2</sub> (L) <sub>3</sub> (NO <sub>3</sub> ) <sub>2</sub> ] <sup>+</sup> (cal. 932.05)		0.101	0.388	0.588	1	0.574	0.287
1335.02	[Dy <sub>3</sub> (L) <sub>4</sub> (NO <sub>3</sub> ) <sub>3</sub> (OH)] <sup>+</sup> (cal. 1335.03)			0.145	0.420	0.839	0.498	0.150
1479.10	[Dy <sub>3</sub> (L) <sub>5</sub> (NO <sub>3</sub> ) <sub>3</sub> ] <sup>+</sup> (cal. 1479.11)			0.103	0.335	0.736	1	1

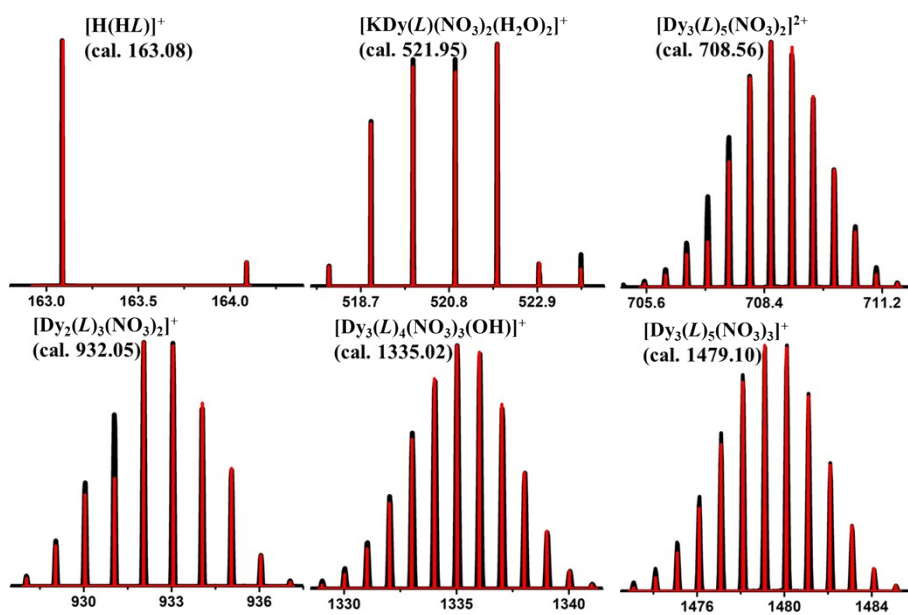


**Figure S16.** The Time-dependent ESI-MS superposed simulated and observed spectra of several species for **1**.